

Title	Metabolic flux and flux balance analyses indicate the relevance of metabolic thermogenesis and aerobic glycolysis in cancer cells
Author(s)	Okahashi, Nobuyuki; Shima, Tomoki; Kondo, Yuya et al.
Citation	Metabolic Engineering. 2025, 92, p. 185-193
Version Type	VoR
URL	https://hdl.handle.net/11094/102861
rights	This article is licensed under a Creative Commons Attribution 4.0 International License.
Note	

# The University of Osaka Institutional Knowledge Archive : OUKA

https://ir.library.osaka-u.ac.jp/

The University of Osaka

ELSEVIER

Contents lists available at ScienceDirect

## Metabolic Engineering

journal homepage: www.elsevier.com/locate/meteng





## Metabolic flux and flux balance analyses indicate the relevance of metabolic thermogenesis and aerobic glycolysis in cancer cells

Nobuyuki Okahashi <sup>a,\*</sup> <sup>o</sup>, Tomoki Shima <sup>a</sup>, Yuya Kondo <sup>a</sup>, Chie Araki <sup>a</sup>, Shuma Tsuji <sup>a</sup>, Akane Sawai <sup>a</sup>, Hikaru Uehara <sup>a</sup>, Susumu Kohno <sup>b</sup>, Hiroshi Shimizu <sup>a</sup>, Chiaki Takahashi <sup>b</sup>, Fumio Matsuda <sup>a,\*\*</sup>

- <sup>a</sup> Department of Bioinformatic Engineering, Graduate School of Information Science and Technology, The University of Osaka, 1-5 Yamadaoka, Suita, Osaka, 565-0871, Japan
- b Cancer Research Institute, Kanazawa University, Kakuma-machi, Kanazawa, Ishikawa, 920-1192, Japan

#### ARTICLE INFO

Keywords: Metabolic flux analysis Flux balance analysis Metabolic heat Aerobic glycolysis Caner metabolism

#### ABSTRACT

Adenosine triphosphate (ATP) regeneration by substrate-level phosphorylation is a general feature of cancer metabolism, even under normoxic conditions (aerobic glycolysis). However, it is unclear why cancer cells prefer inefficient aerobic glycolysis over the highly efficient process of oxidative phosphorylation for ATP regeneration. To investigate the metabolic principles underlying aerobic glycolysis, we performed <sup>13</sup>C-metabolic flux analysis of 12 cultured cancer cell lines and explored the metabolic constraints required to reproduce the results using *in silico* metabolic simulations. We found that the measured flux distribution can be reproduced by maximizing the ATP consumption in the flux balance analysis considering a limitation of metabolic heat dissipation (enthalpy change). Consistent with the simulation, OXPHOS inhibition induced metabolic redirection to aerobic glycolysis while maintaining the intracellular temperature. Furthermore, the dependency on aerobic glycolysis was partly alleviated upon culturing at low temperatures. Our data suggest that metabolic thermogenesis is an important factor in understanding aerobic glycolysis in cancer cells and that an advantage of aerobic glycolysis is the reduction in metabolic heat generation during ATP regeneration.

### 1. Introduction

Adenosine triphosphate (ATP) regeneration is one of the most important metabolic processes and is required to maintain various cellular functions. Generally, normal human cells efficiently regenerate ATP by oxidative phosphorylation (OXPHOS) through the electron transport chain (ETC) (32 ATP/glucose, denoted as the glucose  $\rightarrow$  TCA cycle). In contrast, cancer cells depend on substrate-level phosphorylation for ATP regeneration, even under conditions of oxygen availability (2 ATP/glucose, aerobic glycolysis) (De Berardinis and Chandel, 2016). This altered metabolic state is ascribed to the reduced ETC activity that triggers the metabolic rewiring toward aerobic glycolysis to meet the large ATP demand for active cell proliferation in cancer cells (Koppenol et al., 2011) as well as to supply building blocks for biomass synthesis. However, ETC deficiency depends on the type of cancer cell line as certain cell types activate ETC and more than 50 % of ATP regeneration

is attributed to OXPHOS (Zu and Guppy, 2004). Moreover, cancer cells commonly catabolize glutamine as a carbon source to regenerate ATP by OXPHOS (glutaminolysis) (Fan et al., 2013; Yang et al., 2017). Thus, the rationale for employing aerobic glycolysis for ATP regeneration is far from being understood, although several possible roles have been proposed (Liberti and Locasale, 2016). In this study, we investigated potential factors contributing to the induction of aerobic glycolysis using flux balance and <sup>13</sup>C-metabolic flux analyses, under the assumption that neither oxygen availability nor respiratory capacity is a limiting factor.

#### 2. Results

2.1. <sup>13</sup>C-MFA of 12 cancer cell lines did not show a correlation between total ATP regeneration flux and cell proliferation rates

In this study, we performed <sup>13</sup>C-metabolic flux analysis (<sup>13</sup>C-MFA) of

E-mail addresses: n-okahashi@ist.osaka-u.ac.jp (N. Okahashi), fmatsuda@ist.osaka-u.ac.jp (F. Matsuda).

https://doi.org/10.1016/j.ymben.2025.08.002

Received 7 April 2025; Received in revised form 11 July 2025; Accepted 4 August 2025 Available online 7 August 2025

1096-7176/© 2025 The Authors. Published by Elsevier Inc. on behalf of International Metabolic Engineering Society. This is an open access article under the CC BY license (http://creativecommons.org/licenses/by/4.0/).

<sup>\*</sup> Corresponding author.

<sup>\*\*</sup> Corresponding author.

12 cancer cell lines cultured in  $[1^{-13}C]$ glucose medium and *in silico* metabolic simulations. These cell lines were selected based on the diversity of their expression patterns for genes associated with central carbon metabolism to obtain a global view of energy metabolism (Klijn et al., 2015) (Fig. S1). Their ability to grow in Dulbecco's modified Eagle's medium (DMEM) was considered to reduce the bias derived from the culture conditions. The specific cell proliferation rate, cell adhesion area, and diameter of trypsinized cells were measured as visible phenotypes of the cell cultures (Table S1).

Metabolic flux distributions allowed quantitative comparison of flux levels among pathways (Antoniewicz, 2015; Duckwall et al., 2013) (Fig. 1A and S2, Table S2, Data S1). Details of the procedure for  $^{13}\text{C-MFA}$ are provided in the supplemental Text (Text S1). ATP was mainly regenerated by three metabolic pathways in the 12 cancer cell lines: aerobic glycolysis (red arrow in Fig. 1A), glutaminolysis (blue arrow), and glucose → TCA cycle (gray arrow). Glucose to pyruvate flux, a common feature of aerobic glycolysis, and the glucose → TCA cycle were treated separately under conditions based on the ratio of lactate secretion flux and TCA cycle flux. In the case of MCF-7 cells, the metabolic flux level in glycolysis, represented by the glyceraldehyde-3-phosphate dehydrogenase (GAPDH) reaction, was 1104 nmol  $(10^6 \text{ cells})^{-1} \text{ h}^{-1}$ . The flux levels of glutamate dehydrogenase (GLUDH, representing the glutaminolysis flux) and the isocitrate dehydrogenase (IDH) reaction (representing the glucose → TCA cycle flux) were less than 10 % of the glycolytic flux, that were 19 and 25 nmol  $(10^6 \text{ cells})^{-1} \text{ h}^{-1}$ , respectively (Fig. 1A). All 12 cell lines demonstrated similar trends, that is, the flux through aerobic glycolysis was generally higher than that through glutaminolysis and the glucose → TCA cycle (Fig. S3). However, significant variations were observed in the fluxes of GAPDH, GLUDH, and IDH reactions among the cell lines (Fig. S3). Among these, the glucose → TCA cycle flux was not universal because the metabolic flux levels of the IDH reaction were close to zero in HepG2 and MIA PaCa-2 cells (Fig. S3). Principal component analysis revealed no definite correlation between the metabolic flux distributions and cell origins (Fig. 1B), suggesting that the variations may be due to other biological contexts in each cell line.

Net ATP regeneration rates within the central carbon metabolic network were calculated from the metabolic flux distributions (Fig. 1C). For instance, the net ATP regeneration rate in MCF-7 cells was 1815 nmol  $(10^6 \text{ cells})^{-1} \text{ h}^{-1}$ , which varied 2.8 times among the 12 cell lines.

An approximate estimate indicated that the net ATP regeneration rates were higher than those of most non-cancerous cells (See Supplemental Text S2 for details). Moreover, the ATP regeneration rate in MCF-7 cells showed that 39 % of ATP was regenerated by OXPHOS through the ETC (Fig. 1C). OXPHOS commonly occurred in all 12 cancer cell lines, suggesting that this mechanism is still mandatory for ATP regeneration in cancer cells. Consistent with this observation, the cell lines maintained their mitochondrial membrane potential (Fig. S4). However, a large variation was observed in the OXPHOS-dependent ATP regeneration rate, ranging from 24 % (HepG2) to 68 % (LS174T) of the net ATP regeneration rate (Fig. 1C) (Zhang et al., 2017). This variation is likely to be derived from the distinct ETC activities of each cell line depending on the biological context. Thus, it is reasonable to assume that the ETC must work within an optimal capacity as a loss of mitochondrial membrane potential by low ETC activity triggers cell apoptosis (Li et al., 2003; Ly et al., 2003) and an ETC overload excessively generates reactive oxygen species, which also induces cell apoptosis (Zhao et al., 2019).

Given that cells maintain a rapid turnover of ATP, it can be assumed that an equal amount of regenerated ATP must be consumed for some cellular functions, such as proliferation. However, no correlation was observed between ATP regeneration rates and specific cell proliferation rates (r = 0.06, Fig. 1D and S5), suggesting the presence of other major ATP demands in cultured cancer cells. The correlation analysis indicated that the cell adhesion area on the culture plates was positively correlated with the net ATP regeneration rates (r = 0.76, Fig. 1D and S5). This trend was also observed when an outlier (Caki-1) was removed from the dataset (r = 0.68; Fig. S6). Moreover, no correlation was observed between the cell adhesion area and diameter of the trypsinized floating cells (r = 0.07, Fig. 1D). Thus, the cell adhesion area is a phenotype of cancer cells that is distinct from the cell volume. Notably, the adhesion between the cell and the extracellular matrix mediated by cadherin promotes cancer cell invasion in conjunction with metabolic changes to produce the required amount of ATP (Sousa et al., 2019). Actin and myosin utilize ATP to regulate tumor cell adhesion and migration (Ouderkirk and Krendel, 2014; Zanotelli et al., 2018). Taken together, these results indicate that cancer cell metabolism is not shaped by a proliferation-oriented mechanism.

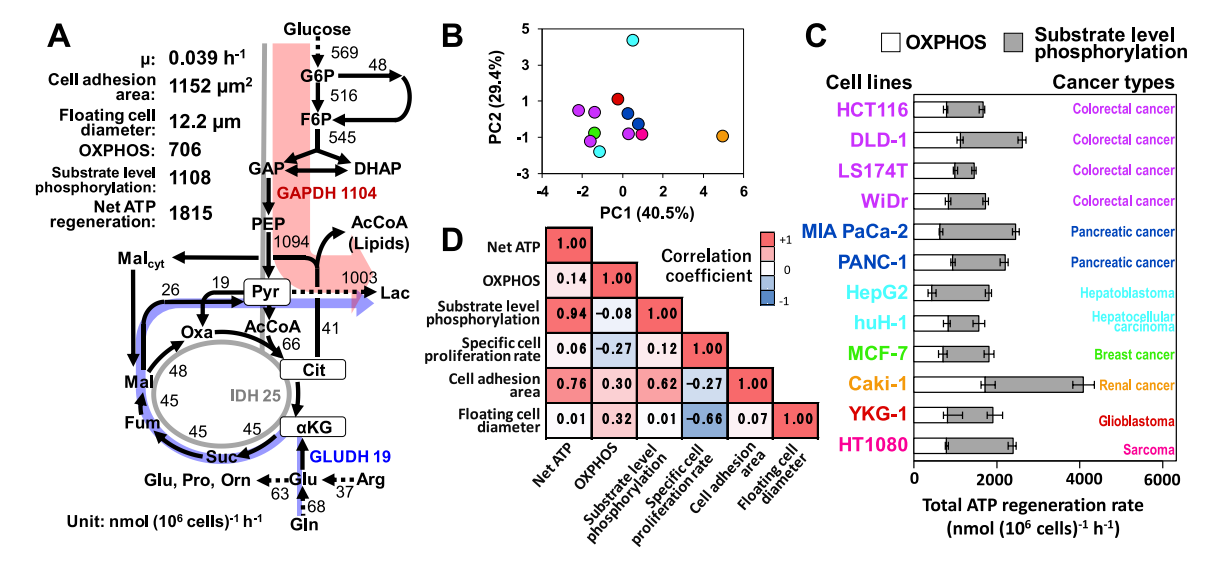


**Fig. 1.** Variation in the metabolic flux distribution among 12 cancer cell lines and their correlation with the phenotypes. **(A)** Metabolic flux distribution of MCF-7 as determined by  $^{13}$ C-MFA. **(B)** The score plot of the principal component analysis using the metabolic flux distributions of 12 cell lines. The color legend is identical to that of the next panel. **(C)** Variations in ATP regeneration rates by substrate-level phosphorylation and OXPHOS. Error bars represent 95 % confidence intervals. **(D)** Correlation between ATP regeneration rates and visible cell phenotypes. Spearman's rank order correlation coefficients are depicted in the heat map (n = 12). (For interpretation of the references to color in this figure legend, the reader is referred to the Web version of this article.)

# 2.2. In silico simulation indicates that aerobic glycolysis is required to reduce metabolic heat

To elucidate the principle underlying the coordination of cancer metabolism, we explored the metabolic constraints required to reproduce the measured flux distributions using *in silico* metabolic simulations. We performed flux balance analysis (FBA) using a genome-scale model of human metabolism (RECON2) (Thiele et al., 2013) (Data S2). FBA requires an objective function to simulate the intracellular metabolic flux distribution using a linear programming method (Feist and Palsson, 2010). Although maximal biomass production is commonly used as an objective function to simulate bacterial metabolism, a suitable objective function for simulating cancer cell metabolism remains under investigation (Zielinski et al., 2017). In this study, the <sup>13</sup>C-MFA results suggested that the cultured cancer cells consumed a large amount of ATP to maintain certain cellular functions other than proliferation (Fig. 1D). Thus, the maximal ATP consumption was employed as the objective function in the *in silico* analysis.

The FBA also requires constraints on the solution space (upper and lower boundaries of the metabolic flux vector) (Orth et al., 2010). Here, we performed FBA to determine additional constraints that drive cell metabolism toward aerobic glycolysis and glutaminolysis for ATP regeneration, as revealed in the <sup>13</sup>C-MFA (Fig. 1). The flux distribution of MCF-7 cells was chosen as an example for reproduction by FBA (Fig. 2A). The relatively minor metabolic fluxes, such as those related to biomass synthesis as well as the uptake and production of amino acids other than glutamine, were constrained at the measured values of MCF-7 (the uncertainty of flux measurements was not considered). Specifically, the largest biomass flux from acetyl-CoA to lipid synthesis accounted for only 8.1 % of glucose uptake, while all other biomass synthesis fluxes were even lower, under 2 %. The rates of arginine uptake and ornithine secretion were 7.3 % and 8.1 % of glucose uptake, respectively, indicating that they were nearly balanced. The uptake rates of branched-chain amino acids were less than 2.6 % of the glucose uptake rate, with the excess assumed to be catabolized for energy production. The essential amino acids were not modeled as their uptake was roughly balanced by the biomass demand (Okahashi et al., 2015). Amino acid secretion was observed for alanine, glutamate, and proline, with secretion rates of 4.3, 3.2, and 0.8 % of glucose uptake, respectively. These calculations verify that biomass synthesis and secretion of non-essential amino acids made only a minor contribution to reproducing the flux distribution of central carbon metabolism (all constraints for the influx and efflux are presented in Table S3). In contrast, no specific constraints were imposed on the uptake rates of glucose, glutamine, and oxygen and the excretion rates of lactate, carbon dioxide, and water.

The FBA results without additional constraints showed that considerable amounts of glucose and glutamine were consumed until the ATP regeneration rate reached the upper limit (Fig. 2B, Data S3). The predicted metabolic flux distribution mainly exhibited OXPHOS-dependent metabolism through the glucose  $\rightarrow$  TCA cycle and a low correlation coefficient with that observed in MCF-7 cells (r=0.62). This indicated that additional constraints are required to reproduce the measured value for MCF-7 cells.

In this study, we considered various thermodynamic parameters that govern cell metabolism (Niebel et al., 2019). For example, the entire stoichiometry of aerobic glycolysis (glucose  $\rightarrow$  2 lactate) indicates that the enthalpy change  $(\Delta_r H^{\circ\circ})$ , or metabolic heat generation, per 1 mol of ATP regeneration by aerobic glycolysis is -55.0 kJ (mol ATP) $^{-1}$  (Table S4) (Alberty, 1998). Similarly, the enthalpy change in the glucose  $\rightarrow$  TCA cycle reaction was -88.2 kJ (mol ATP) $^{-1}$  when proton leak and slip were not considered (Table S4). Thus, it is expected that if the enthalpy change is limited, aerobic glycolysis would be preferentially employed for ATP regeneration in cells. Recent studies have suggested that 8H $^+$ /3ATP-type ATP synthase is also present in humans. Even if all ATP synthase operated in this manner, the enthalpy change would still be -61.3 kJ/mol, which is greater than that of glycolysis. This study employed the theoretical enthalpy change -55.0 kJ (mol ATP) $^{-1}$  for the glucose  $\rightarrow$  TCA cycle reaction. The preference for aerobic glycolysis was

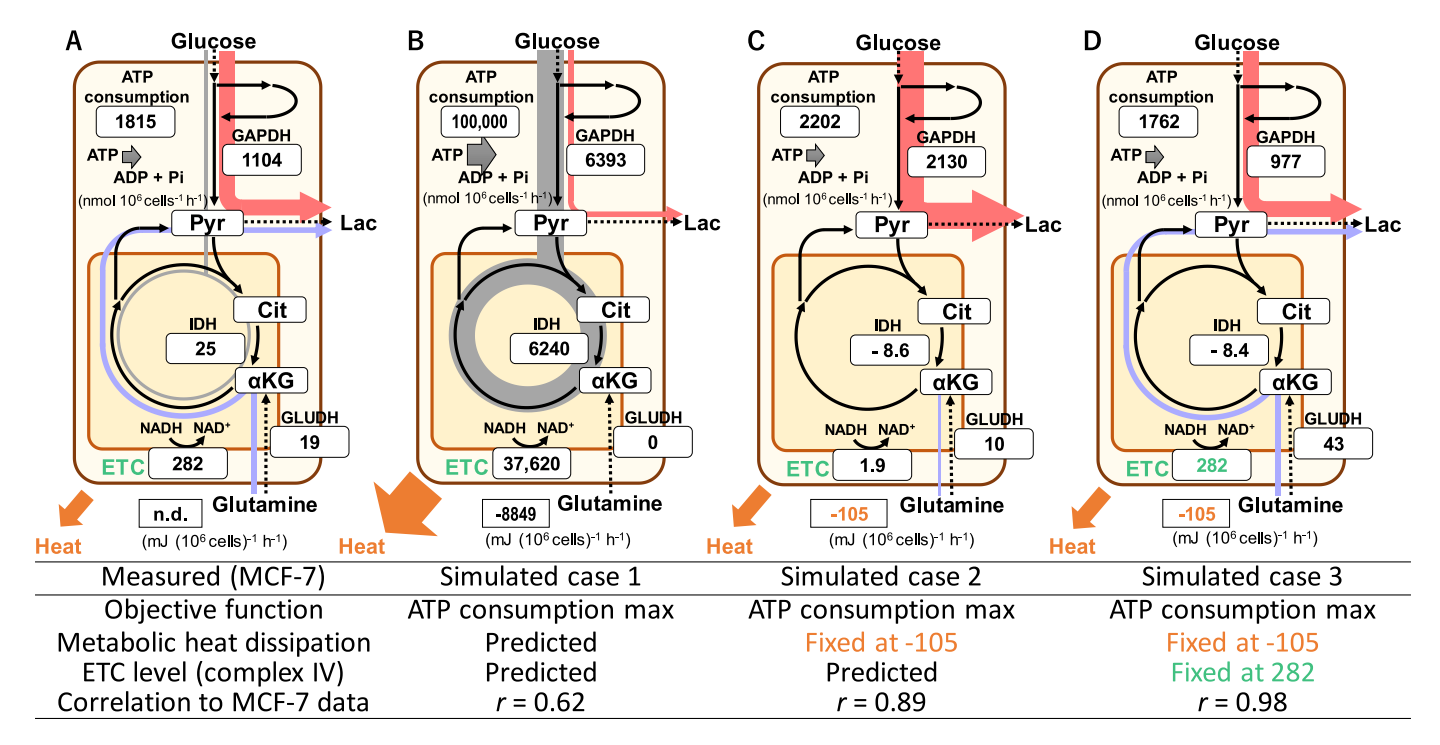


Fig. 2. Metabolic heat dissipation and ETC activity govern cancer cell metabolism. *In silico* simulation of metabolism was performed using the FBA with a genome-scale model of human metabolism (RECON2). Metabolic flux levels of the key reactions of aerobic glycolysis (red), glucose → TCA cycle (gray), and glutaminolysis (blue) are displayed in the boxes. The maximum ATP consumption was employed as an objective function. Additional constraints are represented by yellow and green numbers. (A) Measured metabolic flux distribution in MCF-7 cells. (B−D) Results of FBA (B) without additional constraints, (C) with fixed metabolic heat dissipation, and (D) with fixed metabolic flux dissipation and ETC flux.

not observed for other parameters, such as entropy and Gibbs free energy change (Table S4). Thus, the genome-scale metabolic model was modified to determine the levels of cellular dissipation of enthalpy change from the FBA results (Table S5 and Data S3) (Alberty, 1998).

The FBA was repeatedly performed by fixing the  $\Delta_r H^{\circ}$  level to a range of plausible values as an additional constraint and compared it with the measured flux distribution. We found that when the  $\Delta_r H^{\circ}$  level was set at -105 mJ  $(10^6$  cells) $^{-1}$  h $^{-1}$ , the predicted metabolic flux distribution was more similar to the measured MCF-7 data (Fig. 2C, r=0.89) because aerobic glycolysis was activated for ATP regeneration, as expected.

In addition to metabolic heat, the ETC activity was applied as an additional constraint because the level of ETC flux in the above simulation was considerably low (Fig. 2C), which was inconsistent with the measured data (Fig. 2A and S4). Thus, FBA was performed by fixing the metabolic flux level of complex IV of the ETC at the calculated values from <sup>13</sup>C-MFA data of MCF-7 cells (282 nmol (10<sup>6</sup> cells)<sup>-1</sup> h<sup>-1</sup>). The

predicted metabolic flux distribution successfully reproduced ATP regeneration by both aerobic glycolysis and glutaminolysis, and its correlation with the measured flux distributions was r=0.98 (Fig. 2D, Fig. S7, Data S3). However, ATP regeneration by the glucose  $\rightarrow$  TCA cycle did not occur in the predicted distribution (Fig. 2D), which was inconsistent with the  $^{13}\text{C-MFA}$  result (Fig. 2A). This is because the metabolic heat dissipation per 1 mol of ATP regeneration by glutaminolysis is lower than that of the glucose  $\rightarrow$  TCA cycle reaction, although the detailed  $^-\Delta_r H^{,\circ}$  level cannot be calculated by simple material balance equations. Notably, the glucose  $\rightarrow$  TCA cycle pathway is not universal, as mentioned above (Fig. S3). The FBA showed that similar ATP regeneration occurred by both aerobic glycolysis and glutaminolysis in all 12 cell lines (Fig. S7 and Data S3). The simulation of cancer cell metabolism suggested that the ETC activity and metabolic heat generation are possible constraints of cancer cell metabolism.

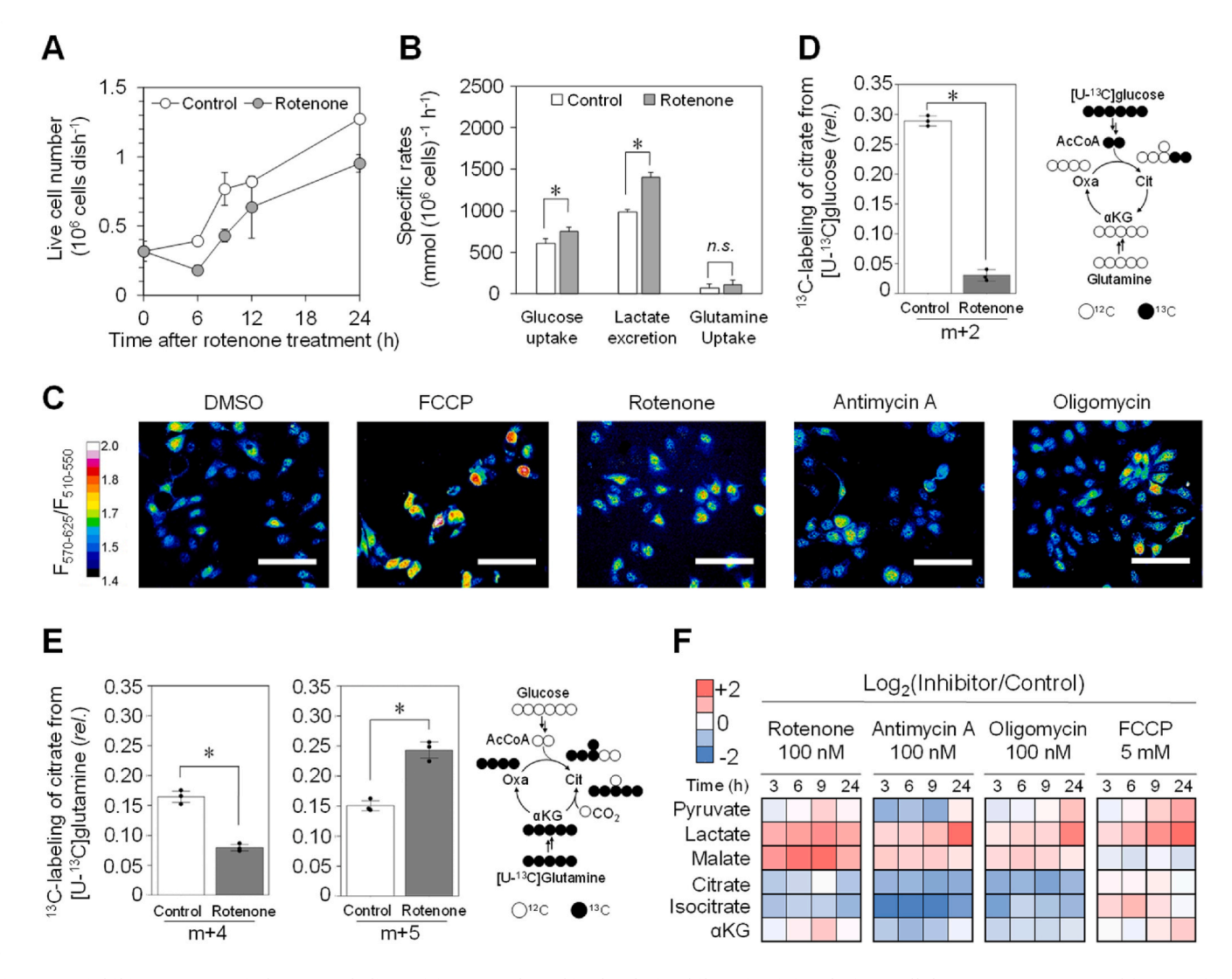


Fig. 3. ETC inhibitor treatment induces metabolic rewiring toward aerobic glycolysis while maintaining the intracellular temperature. (A) Proliferation of MCF-7 cells after 100 nM rotenone treatment. (B) Specific rates for glucose and glutamine uptake and lactate excretion between 12 and 24 h of culturing. Asterisks indicate the statistical significance relative to the control, as determined using a two-sided Student's *t*-test (p < 0.05). (C) Intracellular temperature of MCF-7 treated by ETC-inhibitors for 24 h. Intracellular temperatures of MCF-7 cells treated with DMSO, 100 nM rotenone, 100 nM antimycin, 100 nM oligomycin, and 5 mM FCCP for 24 h were measured using a cellular thermoprobe. The color scale represents the fluorescence intensity ratio (570–625/510–550 nm), which corresponds to the intracellular temperature. (D) M+2 citrate in MCF-7 cells in  $[U_{-}^{13}C]$  glucose tracing (left). Atom mapping of  $[U_{-}^{13}C]$  glucose (right). (E) M+4 and M+5 citrate in MCF-7 cells in  $[U_{-}^{13}C]$  glutamine tracing (left). Atom mapping of  $[U_{-}^{13}C]$  glutamine tracing (left). Atom mapping of metabolites (Log<sub>2</sub> (fold change)) are shown in the heatmap. All data are represented as mean  $\pm$  SD (n = 3). (For interpretation of the references to color in this figure legend, the reader is referred to the Web version of this article.)

# 2.3. ETC inhibitor treatment induces metabolic rewiring toward aerobic glycolysis while maintaining the intracellular temperature

The metabolic simulation indicates that the downregulation of ETC activity will be compensated by the elevation of aerobic glycolysis while maintaining the heat dissipation level, which corresponds to a metabolic shift from the level in Fig. 2D to that in Fig. 2C. We sought to reproduce the results experimentally to validate the result of the metabolic simulation. To downregulate the ETC activity, the MCF-7 cells were treated with a complex I inhibitor, rotenone (100 nM). The time-course data showed that cell proliferation was temporarily halted by 6 h and then recovered between 6 and 24 h (Fig. 3A). The recovery in growth was accompanied by the activation of aerobic glycolysis as the specific rates for glucose consumption and lactate production between 12 and 24 h increased by 1.2-fold with rotenone treatment (Fig. 3B). Our previous study has also demonstrated that treatment with other ETC inhibitors, antimycin A (complex III) and oligomycin (ATP synthase), similarly increased specific rates of glucose uptake and lactate production in MCF-7 cells (Sawai et al., 2025). These experiments adequately reflected the metabolic shift from Fig. 2D to Figure 2C predicted by FBA.

To evaluate the effect of changes in heat generation by the metabolic redirection, the intracellular temperature of cells treated with ETC inhibitors was measured using a cellular thermoprobe (Uchiyama et al., 2017) (see Materials and methods section). As a positive control, the intracellular temperature of MCF-7 treated with the mitochondrial uncoupler carbonyl cyanide 4-(trifluoromethoxy)phenylhydrazone (FCCP) was measured. As expected, the temperature increase resulting from hyperactivation of the ETC and the TCA cycle induced by FCCP was accurately captured (Fig. 3C). In contrast, treatment with rotenone and other ETC inhibitors, including antimycin A and oligomycin, did not significantly change the intracellular temperature, demonstrating that aerobic glycolysis was elevated while maintaining the heat dissipation level (Fig. 3C). The increased glucose uptake and lactate secretion rates within the heat dissipation capacity, as observed with ETC inhibitor treatments (Fig. 3B), were reproduced by metabolic simulation that restricted ETC activity (Fig. 2C compared to Fig. 2D), supporting the validity of the metabolic model considering enthalpy change.

To estimate the switching point at which metabolic rewiring is induced by ETC inhibition,  $^{13}\text{C-tracer}$  and metabolome analysis were performed. Tracer analysis using [U-13C]glucose demonstrated that an m+2 isotopomer of citrate, which is produced from m+2 acetyl-CoA and unlabeled oxaloacetate, was reduced after rotenone treatment (Fig. 3D). [U-13C]glutamine tracing also revealed that the relative abundance of the m+4 citrate was reduced after rotenone treatment, whereas that of m+5 citrate produced by reductive glutamine metabolism increased (Fig. 3E). The labeling pattern indicated a reduction in the flux of the glucose → TCA cycle in the rotenone-treated MCF-7 cells, consistent with the result of metabolic simulation (Fig. 2C compared to Fig. 2D). Metabolome analysis showed that rotenone treatment induced an accumulation of malate and lactate, while also decreasing the citrate and isocitrate levels (Fig. 3F), suggesting the suppression of entry reaction of the TCA cycle, such as citrate synthase, pyruvate dehydrogenase (PDH), and/or pyruvate transport from cytosol to mitochondria. A similar metabolic profile was commonly induced by ETC inhibitors antimycin A (complex III) and oligomycin (APT synthase), possibly due to TCA cycle stagnation resulting from OXPHOS inhibition (Fig. 3F) (Zhang et al., 2021), but not by FCCP, which activates the TCA cycle, unlike ETC inhibitors (Fig. 3F) (Si et al., 2009). Inhibition at the TCA cycle entry point is consistent with previous knowledge that PDH activity is suppressed via hypoxia-induced factor-1-mediated PDH kinase under anaerobic conditions (Kim et al., 2006). These results suggest that the downregulation of the entry point of the TCA cycle is one of the contributing factors to a metabolic shift from the glucose → TCA cycle to aerobic glycolysis.

# 2.4. Metabolic rewiring toward aerobic glycolysis is dependent on temperature

The above observations suggest that cancer cells rewire their metabolism to control the heat dissipation level. The glucose  $\rightarrow$  TCA cycle pathway is preferable and unfavorable under lower and higher temperature conditions, respectively, to maintain a constant intracellular temperature. To test this assumption, cells were cultured at control (37 °C), low (36 °C), and high (38 °C) temperatures. A comparison between the glucose and lactate consumption for 18 h showed that there was a limited effect on the glucose consumption (Fig. 4A), whereas lactate production tended to decrease and increase at 36 and 38 °C, respectively (Fig. 4B). A significant increase in lactate production was observed in both cell lines at 38 °C (*t*-test,  $n=3, \alpha=0.05$ ). In contrast, a significant decrease in lactate production was observed in five cell lines at 36 °C. The significance of changes in lactate/glucose yield was not confirmed (Fig. 58). These results indicated that aerobic glycolysis was temperature-sensitive.

Gene expression data were obtained from MCF-7 and HCT116 cells, which indicated a temperature-dependent increase in lactate production, as representative cell lines (n = 1, Table S6, Data S4). We selected a total of 3154 and 4533 open reading frames (ORFs), whose expression levels were altered in MCF-7 and HCT116 cells in the following order: [36 °C]>[37 °C]>[38 °C]. A total of 683 ORFs were common in the MCF-7 and HCT116 datasets (Fig. 4C, Data S5), which was significantly larger than the expected number of overlapping ORFs (545 ORFs,  $\chi^2$  test, p-value =  $2.0 \times 10^{-9}$ ). An over-representation analysis was performed for the 683 ORFs using the Kyoto Encyclopedia of Genes and Genomes (KEGG) 2019 human dataset (Xie et al., 2021). The results revealed that ORFs in the "TCA cycle" category (PDHA1, MDH2, IDH3G, IDH3B, OGDHL, DLAT, and SDHD) and "Pyruvate metabolism" category (ALDH3A2, LDHA, PDHA1, MDH2, DLAT, and ALDH7A1) were enriched in 683 ORFs (Fig. 4D-Table S7). Notably, PDHA1 and DLAT encode subunits of the pyruvate dehydrogenase complex, which is located at the entry point of the TCA cycle; this was also indicated in the aforementioned metabolome analysis (Fig. 3F). No functional category was found in the ORF list that exhibited a reversed expression pattern in the following order: [36  $^{\circ}\text{C}]{<}[37\ ^{\circ}\text{C}]{<}[38\ ^{\circ}\text{C}]$  (data not shown). These results suggest that metabolic rewiring from the glucose  $\rightarrow$  TCA cycle to aerobic glycolysis is dependent on temperature-induced changes in the metabolic thermogenesis.

### 3. Discussion

Thermogenesis has long been observed in patients with breast cancer (Cavaliere et al., 1967). This implies that the cancer tissue generates additional heat by activation of metabolism to meet the elevated ATP demand, such as rapid cell proliferation, tumor cell adhesion, and migration. This study reaffirms that thermogenesis is an important aspect of cellular metabolism, particularly when cancer cells require large amounts of ATP. We showed that the active use only of the TCA cycle and OXPHOS pathway leads to unfeasibly excessive metabolic heat generation. Heat generated in the TCA cycle is derived from the enthalpy changes of the metabolic reaction, which differs from the thermogenesis mediated by uncoupling proteins. In contrast to the activation of the OXPHOS pathway, the additional use of aerobic glycolysis can compensate for the lack of ATP, which limits cellular thermogenesis in the glucose → TCA cycle. This is a plausible scenario for ATP production in cancer cells, as all 12 cancer cell lines investigated in this study employed aerobic glycolysis in combination with OXPHOS. Thus, cell metabolism operates within an appropriate range of metabolic heat generation. Under the condition that oxygen availability and respiratory capacity are not limiting factors, it is suggested that thermogenesis is an additional constraint in modeling cancer cell metabolism. Previous studies have proposed various explanations for the deviations from the optimum metabolism in mammalian cells and benefits of aerobic

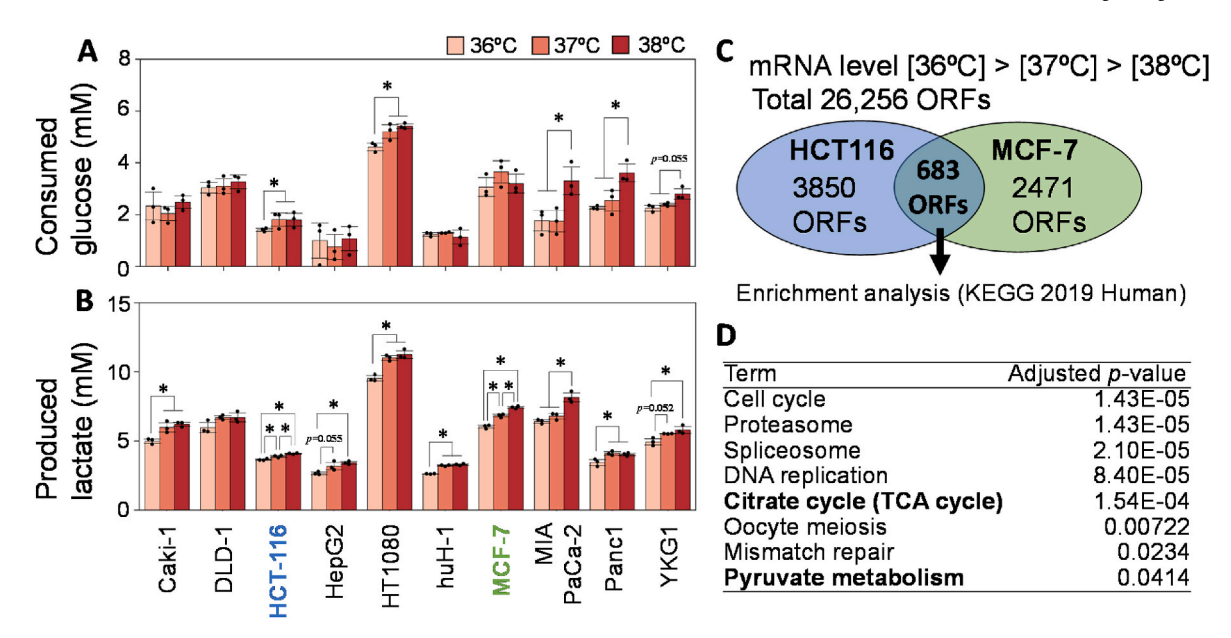


Fig. 4. Culture temperature induces metabolic rewiring by altering gene expression. Cancer cells were cultured under control (37 °C), low (36 °C), and high (38 °C) temperatures. Concentrations of **(A)** consumed glucose and **(B)** produced lactate in the culture medium at 18 h. Data are represented as mean  $\pm$  SD (n=3). Asterisks indicate the statistical significance of concentrations under test conditions as determined by one way analysis of variance (ANOVA) using the Tukey-Kramer method (\*p < 0.05). **(C)** Venn diagram of temperature-responsive genes. RNA-Seq of MCF-7 and HCT116 cells at 24 h identified 3154 and 4533 genes expressed with fold changes in the following order: [36 °C]>[37 °C]>[38 °C]. **(D)** An over-represented analysis of gene categories of 683 common genes by Enricher using the KEGG 2019 Human dataset (Xie et al., 2021).

glycolysis, such as satisfying rapid energetic demand (Epstein et al., 2014), protein allocation and efficiency (Chen and Nielsen, 2019; Elsemman et al., 2022), and limitation of mitogenesis and mitochondrial activity (Arunachalam et al., 2024; Fernandez-De-Cossio-Diaz and Vazquez, 2017). Our study has added another factor that makes aerobic glycolysis favorable for cells, and the relevance between the factors proposed so far and metabolic thermogenesis will be an issue to be investigated.

Although the association between heat and metabolism was elucidated in *in silico* simulations (Fig. 2) and in metabolome analysis (Fig. 3F), it resulted in a minor impact on lactate yield in culture experiments at low and high temperatures (Fig. S8). A possible course is the differences in the magnitude of the fluxes (Fig. 1A); the flux from pyruvate to acetyl-CoA (66 nmol/ $10^6$  cells/h) is much smaller than the lactate secretion flux (1003 nmol/ $10^6$  cells/h). Another factor is the difficulty of accurately measuring glucose levels for calculating yield (Tanner et al., 2018). Hence, it is reasonable to consider that both the activation of glycolysis flux itself and the redirection of the flux from the TCA cycle to lactate may contribute to aerobic glycolysis.

The mechanisms whereby cells sense temperature and coordinate metabolism are still lacking. One possibility is the temperaturedependent alteration of phospholipid acyl chain properties (Murakami et al., 2022). Murakami et al. showed that intracellular temperature can be maintained by  $\Delta 9$ -fatty acid desaturase DESAT1 in Drosophila S2 cells. Acyl chain desaturation leads to the activation of F1F0-ATPase and regulation of intracellular temperature homeostasis via transformation of mitochondrial structures, indicating that external heat radiation regulates respiration, as demonstrated by hyperthermia (Cavaliere et al., 1967). These results provide new insights into the relevance of cancer metabolism to malignancy, cancer microenvironment interactions, and drug resistance (Liberti and Locasale, 2016). Heat generation may also contribute to the activation of immune cells and regulation of the cancer microenvironment (Kokolus et al., 2013; Repasky et al., 2013). Furthermore, the relationship between metabolism and heat is universal. Notably, aerobic glycolysis has been observed in normal cells, including astrocytes, embryos, and stem cells (Abe et al., 2006; Ito and Suda, 2014; Miyazawa et al., 2017). These cell types and their tissues commonly require large amounts of ATP for biochemical processes. However, embryos lacking vasculature have limited heat release capacity. The role of aerobic glycolysis in cancer and normal cells, in relation to their mechanisms for maintaining heat homeostasis, should be further analyzed.

#### 4. Materials and methods

#### 4.1. Cell lines and culture conditions

Twelve human cancer cell lines derived from colorectal cancer (HCT116, DLD-1, LS174T, and WiDr), pancreatic cancer (MIA Paca-2 and PANC-1), hepatoblastoma (HepG2), hepatocellular carcinoma (huH-1), breast cancer (MCF-7), renal cancer (Caki-1), glioblastoma (YKG-1), and sarcoma (HT1080) were obtained from the RIKEN Bioresource Research Center and Japanese Collection of Research Bioresources (JCRB) Cell Bank. Culture experiments were conducted as described previously (Okahashi et al., 2015, 2019). In particular,  $1.0 \times$ 10<sup>6</sup> cells were seeded in 10 mL of Dulbecco's modified Eagle's medium (DMEM) supplemented with 10 % fetal bovine serum (FBS) and 1 % penicillin/streptomycin (Wako) in 100-mm (diameter) plates and cultured for 15 h at 37 °C under 5 %  $\rm CO_2$ .  $^{13}$ C-labeling was performed in 10 mL of DMEM containing 20 mM [ $\rm 1^{-13}C$ ] of glucose (Cambridge Isotope Laboratories, Andover, MA, USA, over 99 % purity) and 10 % dialyzed FBS (Life Technologies, Gaithersburg, MD, USA). The cells were counted noninvasively at 0, 12, 16, 20, and 24 h in triplicate cultures using a CKX53 inverted microscope (Olympus, Tokyo, Japan) equipped with a DP22 digital camera (Olympus) and CKX-CCSW software (Olympus). Cell images were obtained at 10 different locations in the culture dish, and the average cell numbers were used to generate the growth curve. Culture media (200  $\mu$ L) were sampled at each time point. Trypsin was added to the plates and activated at 37 °C for 1 min to measure the diameter of the floating cells. After cell collection, the diameter of live cells was counted using trypan blue staining and a TC20 automated cell counter (Bio-Rad, Hercules, CA, USA). Cell sizes were analyzed using the ImageJ software (National Institutes of Health, Bethesda, MD, USA).

#### 4.2. Extracellular metabolite measurements

The collected culture medium was mixed with an equal volume of 20 mM pimelate solution (internal standard) and filtered through a filter cartridge (pore size of 0.45 µm). Glucose, lactate, and acetate concentrations were determined by high-performance liquid chromatography (HPLC) equipped with a refractive index detector (Prominence, Shimadzu, Kyoto, Japan) and an Aminex HPX-87H column (Bio-Rad), as previously described (Okahashi et al., 2015). Amino acid concentrations in the culture media were measured by HPLC using the AccQ.Tag method (Armenta et al., 2010). HPLC Prominence (Shimadzu) system equipped with a Luna C18 (2) column (250 mm, 4.6 mm, and 5.0  $\mu$ m, SHIMADZU GLC, Kyoto, Japan) and a photodiode array detector (260 nm) was used. Derivatized amino acids were eluted with a 20 mM sodium acetate solution containing 0.04 % (v/v) of trimethylamine and phosphate adjusted to a pH of 6.8 (A) and acetonitrile (B) under the following gradient conditions: 0 min, 0 % (B); 0.5 min, 8 % (B), 17.5 min, 12 % (B), 19 min, 15 % (B), 20 min, 20 % (B), 30.6 min, 100 % (B), and 33.1 min, 0 % (B) at a flow rate of 1.0 mL/min. The column oven temperature was maintained at 40 °C.

#### 4.3. Extraction and derivatization of intracellular metabolites

Intracellular metabolites were extracted using the methanol/water/chloroform method (Okahashi et al., 2015). Cellular metabolites were rapidly quenched by adding 800  $\mu L$  of precooled methanol after rapid medium removal and rinsing with phosphate-buffered saline (1 mL). This procedure was performed within 15 s. Cells and solutions were collected by scraping. Cell lysates were transferred into fresh sample tubes, followed by the addition of 800  $\mu L$  of cold chloroform and 320  $\mu L$  of cold water. After vortexing and centrifugation, 250  $\mu L$  of the upper aqueous layer was collected and dried in a vacuum concentrating centrifuge (CVE-3110; Eyela, Tokyo, Japan) at room temperature. The dried metabolites were methoxyaminated and tert-butyldimethylsilyated for gas chromatography-mass spectrometry (GC-MS) analysis, as described previously (Araki et al., 2018). The data for inhibitor treatment after 3h was obtained from our previous study (Sawai et al., 2025).

### 4.4. Gas chromatography/mass spectrometry analysis

Gas chromatography/mass spectrometry (GC/MS) analysis was performed using a GCMS-QP2020 instrument (Shimadzu) equipped with a DB-5MS capillary column (Agilent Technologies). GC/MS was operated under electron impact (EI) ionization at 70 eV. One microliter of the sample was injected at 250 °C using helium as the carrier gas at a flow rate of 1 ml/min. To analyze central metabolite derivatives, the GC oven temperature was maintained at 60 °C, and then increased to 325 °C at 10 °C/min for a total run time of approximately 30 min. The MS source and quadrupole were maintained at 230 and 150 °C, respectively. The effects of naturally occurring isotopes were corrected (Okahashi et al., 2022).

## 4.5. 13C-metabolic flux and mass balance analyses

The specific uptake and secretion rates of extracellular metabolites were calculated as previously described (Matsuda et al., 2017). The metabolic flux distribution was estimated by minimizing the variance-weighted residual sum of squares of measured and estimated mass isotopomer distributions of intracellular metabolites and effluxes using mfapy (Matsuda et al., 2021; Okahashi et al., 2019). The net ATP regeneration flux was calculated using flux distributions and the following assumptions: the reactions catalyzed by hexokinase, phosphofructokinase, pyruvate carboxylase, acetyl-coenzyme A citrate lyase/phosphoglycerate kinase, pyruvate kinase, and succinyl-coenzyme A lyase were assumed to be ATP consuming/regenerating reactions, respectively. NADPH is also assumed to be regenerated in reactions

involving glucose 6-phosphate dehydrogenase, 6-phosphogluconate dehydrogenase, isocitrate dehydrogenase, and malate NADP<sup>+</sup> oxidore-ductase, and NADPH is consumed in the fatty acid and proline biosynthesis pathways. The excess regenerated NADPH was not balanced, assuming that it would be used to detoxify reactive oxygen species. NADH is regenerated in reactions involving glyceraldehyde-3 phosphate dehydrogenase, pyruvate dehydrogenase, alpha-ketoglutarate dehydrogenase, malate dehydrogenase, and transhydrogenase reactions and is consumed by lactate dehydrogenase. We assumed that excess NADH was converted to ATP through OXPHOS. The P/O ratio is assumed to be 2.5. Although FADH<sub>2</sub> was also converted to ATP during OXPHOS, the P/O ratio was assumed to be 1.5. The ATP required for cell biomass synthesis was assumed to be 35 mmol/g of the dry cell weight (Thiele et al., 2013).

#### 4.6. Clustering analysis

The gene expression dataset (E-MTAB-2706) of cancer cell lines was obtained from ArrayExpress (https://www.ebi.ac.uk/arrayexpress/) (Klijn et al., 2015). Genes related to central metabolism were obtained from the KEGG pathway database (glycolysis/gluconeogenesis, pentose phosphate pathway, citrate cycle, D-glutamine and D-glutamate metabolism, and related transporters). The 62 genes were selected because the dataset did not contain missing data. The transcript per million (TPM)-normalized, log<sub>2</sub>-transformed, and Z-scored gene expression datasets of 622 cancer cell lines were used for hierarchical clustering using the Seaborn clustermap of Python 3.8 (Ward method combined with Euclidean distance).

#### 4.7. Flux balance analysis

A human genome-scale model (RECON2) (Thiele et al., 2013) was used with the following modifications: i) 41 reactions responsible for the degradation of essential amino acids were removed from the model as their uptake rates were roughly balanced with the biomass demand (Okahashi et al., 2015); ii) terms of standard enthalpy of formation (MegaJ mol<sup>-1</sup>) were added to intra/extracellular transport reactions (Tables S7 and S8); and iii) the reaction (R\_ent) was added to the sum of the standard enthalpy of formation. The metabolic heat dissipation (hout) was calculated using the following equation:

$$h_{out} = -\left(\sum_{i} \Delta_{f} {H^{\prime}}_{i}^{0} J_{i} - \sum_{i} \Delta_{f} {H^{\prime}}_{j}^{0} J_{j}
ight)$$

Here, Ji and Jj indicate the uptake and excretion flux levels of the ith and jth metabolite, respectively. Moreover,  $\Delta_i H^{0}$  is the standard enthalpy of formation of each metabolite;  $\Delta_i H^{0}$  values at a pH of 7.0 and ion strength of 0.1 M were obtained from published literature (Alberty, 1998). The  $\Delta_i H^{0}$  level of biomass was approximated based on the data from yeast (Popovic, 2019). The approximation did not affect the FBA in this study because the metabolic flux levels for biomass synthesis were fixed at the measured values. FBA was performed using an in-house Python script with the GNU Linear Programming Kit (GLPK) in the pulp module as a linear programming solver.

### 4.8. RNA-sequencing

The total RNA was extracted using the QIAzol lysis reagent (QIA-GEN). Library preparation was performed using the TruSeq stranded mRNA sample prep kit (Illumina, San Diego, CA, USA) according to the manufacturer's instructions. Sequencing was performed on an Illumina HiSeq 3000 platform in the 101 bp single-end mode. Illumina Casava1.8.2 software was used for base calling. Sequenced reads were mapped to the human reference genome sequences (hg19) using TopHat v2.0.13 in combination with Bowtie2 ver. 2.2.3 and SAMtools ver. 0.1.19. Fragments per kilobase of exon per million mapped fragments

(FPKMs) were calculated using Cufflinks version 2.2.1. Gene enrichment analysis was conducted using the Enrichr web tool (Xie et al., 2021).

#### 4.9. Fluorescence microscopy

Cells were seeded on glass bottom plates (35 mm diameter, Matsunami Glass, Osaka, Japan) and stained according to the manufacturer's protocol. The mitochondria were stained using MitoBright LT Red (Dojindo, Kumamoto, Japan). The mitochondrial membrane potential was detected using the JC-1 MitoMP Detection Kit (Dojindo). ECLIPSE TE2000-E inverted microscope (Nikon, Tokyo, Japan) equipped with an oil immersion objective lens (Plan Apo 60 × /1.4 Oil Ph3 DM, Nicon), filter sets (excitation filter, 465-496 nm; emission filter, 515-555; dichroic mirror, 505, Nicon), and an iXon EMCCD camera (Andor Technology Ltd, Belfast, UK) were used. The intracellular temperature was measured using a cellular thermoprobe for fluorescence ratio (Uchiyama et al., 2017) (Funakoshi, Tokyo, Japan). IX71 inverted microscope (Olympus, Tokyo, Japan) equipped with an objective lens (LCPlanFl 20 × /0.40 Ph1, Olympus) and ORCA-Spark digital CMOS camera (Hamamatsu) were used. Fluorescence images were taken using U-MWIBA3 (excitation filter, 460–495 nm; emission filter, 510–550 nm; dichroic mirror, 505 nm. Olympus) and custom-made (excitation filter. 460-495 nm; emission filter, 570-625 nm; dichroic mirror, 505 nm, Olympus) filter cubes. The temperature and CO<sub>2</sub> content of cells were maintained at 37 °C and 5 %, respectively, using a microscope incubator (BLAST, Kawasaki, Japan). Images were analyzed using the ImageJ

#### CRediT authorship contribution statement

Nobuyuki Okahashi: Writing – review & editing, Writing – original draft, Visualization, Validation, Supervision, Software, Investigation, Funding acquisition, Formal analysis, Data curation, Conceptualization, Methodology, Project administration. Tomoki Shima: Investigation, Formal analysis, Data curation. Yuya Kondo: Investigation, Formal analysis, Data curation. Chie Araki: Investigation, Formal analysis, Data curation. Shuma Tsuji: Investigation, Formal analysis, Data curation. Akane Sawai: Investigation, Formal analysis, Data curation. Hikaru Uehara: Investigation, Formal analysis, Data curation. Susumu Kohno: Writing - review & editing, Supervision, Conceptualization, Investigation, Methodology. Hiroshi Shimizu: Writing - review & editing, Supervision, Conceptualization, Methodology. Chiaki Takahashi: Writing review & editing, Supervision, Conceptualization, Methodology. Fumio Matsuda: Writing - review & editing, Writing - original draft, Visualization, Supervision, Software, Investigation, Funding acquisition, Formal analysis, Data curation, Methodology, Project administration, Validation.

## Data materials, and software availability

RNA-Seq data is available at DDBJ of the National Institute of Genetics (https://www.ddbj.nig.ac.jp/index-e.html) via the index of DRA012975. The code to perform the flux balance analyses is deposited on GitHub (https://github.com/fumiomatsuda/FBA-of-cancer-cell-lines).

#### **Competing interests**

Authors declare that they have no competing interests.

#### Acknowledgments

We acknowledge the NGS core facility of the Genome Information Research Center at the Research Institute for Microbial Diseases, The University of Osaka for their support in RNA sequencing and data analysis. We thank Prof. Shinya Kuroda, Dr. Satoshi Ohno (University of Tokyo), and Shimpei Kawaoka (Kyoto University) for helpful comments on this manuscript. We also thank Keiko Fukamoto of the University of Osaka for her skillful technical support. This work was partially supported by JSPS KAKENHI (grant number 20K15100) and Extramural Collaborative Research Grant of Cancer Research Institute, Kanazawa University for N.O., and Grant-in-Aid for Scientific Research on Innovative Areas (Grant no. 17H06303) for F.M.

#### Appendix A. Supplementary data

Supplementary data to this article can be found online at https://doi.org/10.1016/j.ymben.2025.08.002.

#### References

- Abe, T., Takahashi, S., Suzuki, N., 2006. Oxidative metabolism in cultured rat astroglia: effects of reducing the glucose concentration in the culture medium and of Daspartate or potassium stimulation. J. Cerebr. Blood Flow Metabol. 26, 153–160. https://doi.org/10.1038/sji.jcbfm.9600175.
- Alberty, R.A., 1998. Calculation of standard transformed Gibbs energies and standard transformed enthalpies of biochemical reactants. Arch. Biochem. Biophys. 353, 116–130. https://doi.org/10.1006/abbi.1998.0638.
- Antoniewicz, M.R., 2015. Methods and advances in metabolic flux analysis: a minireview. J. Ind. Microbiol. Biotechnol. 42, 317–325. https://doi.org/10.1007/ s10295-015-1585-x
- Araki, C., Okahashi, N., Maeda, K., Shimizu, H., Matsuda, F., 2018. Mass spectrometry-based method to study inhibitor-induced metabolic redirection in the central metabolism of cancer cells. Mass Spectrom. 7, 1–9. https://doi.org/10.5702/massspectrometry.A0067.
- Armenta, J.M., Cortes, D.F., Pisciotta, J.M., Shuman, J.L., Blakeslee, K., Rasoloson, D., Ogunbiyi, O., Sullivan, D.J., Shulaev, V., 2010. Sensitive and rapid method for amino acid quantitation in malaria biological samples using AccQ.Tag ultra performance liquid chromatography-electrospray ionization-MS/MS with multiple reaction monitoring. Analytical Chemistry 82 (2), 548–558. https://doi.org/10.1021/ac9017900.
- Arunachalam, E., Keber, F.C., Law, R.C., Kumar, C.K., Shen, Y., Park, J.O., Wühr, M., Needleman, D.J., 2024. Robustness of mitochondrial biogenesis and respiration explain aerobic glycolysis. https://doi.org/10.1101/2024.07.04.601975.
- Cavaliere, R., Ciocatto, E.C., Giovanella, B.C., Heidelberger, C., Johnson, R.O., Margottini, M., Mondovi, B., Moricca, G., Rossi-Fanelli, A., 1967. Selective heat sensitivity of cancer cells. Biochemical and clinical studies. Cancer 20, 1351–1381. https://doi.org/10.1002/1097-0142(196709)20:9<1351::AID-CNCR2820200902>3.0.CO.
- Chen, Y., Nielsen, J., 2019. Energy metabolism controls phenotypes by protein efficiency and allocation. Proc. Natl. Acad. Sci. U. S. A. 116, 17592–17597. https://doi.org/ 10.1073/nnas.1906569116.
- De Berardinis, R.J., Chandel, N.S., 2016. Fundamentals of cancer metabolism. Sci. Adv. 2. https://doi.org/10.1126/sciadv.1600200.
- Duckwall, C.S., Murphy, T.A., Young, J.D., 2013. Mapping cancer cell metabolism with (13)C flux analysis: recent progress and future challenges. J. Carcinog. 12, 13. https://doi.org/10.4103/1477-3163.115422.
- Elsemman, I.E., Rodriguez Prado, A., Grigaitis, P., Garcia Albornoz, M., Harman, V., Holman, S.W., van Heerden, J., Bruggeman, F.J., Bisschops, M.M.M., Sonnenschein, N., Hubbard, S., Beynon, R., Daran-Lapujade, P., Nielsen, J., Teusink, B., 2022. Whole-cell modeling in yeast predicts compartment-specific proteome constraints that drive metabolic strategies. Nat. Commun. 13. https://doi.org/10.1038/s41467-022-28467-6.
- Epstein, T., Xu, L., Gillies, R.J., Gatenby, R.A., 2014. Separation of metabolic supply and demand: aerobic glycolysis as a normal physiological response to fluctuating energetic demands in the membrane. Cancer Metab 2. https://doi.org/10.1186/ 2004.2002.2.7
- Fan, J., Kamphorst, J.J., Mathew, R., Chung, M.K., White, E., Shlomi, T., Rabinowitz, J. D., 2013. Glutamine-driven oxidative phosphorylation is a major ATP source in transformed mammalian cells in both normoxia and hypoxia. Mol. Syst. Biol. 9, 712. https://doi.org/10.1038/msb.2013.65.
- Feist, A.M., Palsson, B.O., 2010. The biomass objective function. Curr. Opin. Microbiol. 13, 344–349.
- Fernandez-De-Cossio-Diaz, J., Vazquez, A., 2017. Limits of aerobic metabolism in cancer cells. Sci. Rep. 7. https://doi.org/10.1038/s41598-017-14071-y.
- Ito, K., Suda, T., 2014. Metabolic requirements for the maintenance of self-renewing stem cells. Nat. Rev. Mol. Cell Biol. https://doi.org/10.1038/nrm3772.
- Kim, J.W., Tchernyshyov, I., Semenza, G.L., Dang, C.V., 2006. HIF-1-mediated expression of pyruvate dehydrogenase kinase: a metabolic switch required for cellular adaptation to hypoxia. Cell Metab. 3, 177–185. https://doi.org/10.1016/j. cmet 2006.02.002
- Klijn, C., Durinck, S., Stawiski, E.W., Haverty, P.M., Jiang, Z., Liu, H., Degenhardt, J., Mayba, O., Gnad, F., Liu, J., Pau, G., Reeder, J., Cao, Y., Mukhyala, K., Selvaraj, S.K., Yu, M., Zynda, G.J., Brauer, M.J., Wu, T.D., Gentleman, R.C., Manning, G., Yauch, R. L., Bourgon, R., Stokoe, D., Modrusan, Z., Neve, R.M., de Sauvage, F.J., Settleman, J., Seshagiri, S., Zhang, Z., 2015. A comprehensive transcriptional portrait of human cancer cell lines. Nat. Biotechnol. 33, 306–312. https://doi.org/10.1038/nbt.3080.

- Kokolus, K.M., Capitano, M.L., Lee, C.T., Eng, J.W.L., Waight, J.D., Hylander, B.L., Sexton, S., Hong, C.C., Gordon, C.J., Abrams, S.I., Repasky, E.A., 2013. Baseline tumor growth and immune control in laboratory mice are significantly influenced by subthermoneutral housing temperature. Proc. Natl. Acad. Sci. U. S. A. 110, 20176–20181. https://doi.org/10.1073/pnas.1304291110.
- Koppenol, W.H., Bounds, P.L., Dang, C.V., 2011. Otto Warburg's contributions to current concepts of cancer metabolism. Nat. Rev. Cancer 11, 325–337. https://doi.org/ 10.1038/nrc3038
- Li, N., Ragheb, K., Lawler, G., Sturgis, J., Rajwa, B., Melendez, J.A., Robinson, J.P., 2003. Mitochondrial complex I inhibitor rotenone induces apoptosis through enhancing mitochondrial reactive oxygen species production. J. Biol. Chem. 278, 8516–8525. https://doi.org/10.1074/jbc.M210432200.
- Liberti, M.V., Locasale, J.W., 2016. The warburg effect: how does it benefit cancer cells? Trends Biochem. Sci. 41, 211–218. https://doi.org/10.1016/j.tibs.2015.12.001.
- Ly, J.D., Grubb, D.R., Lawen, A., 2003. The mitochondrial membrane potential (δψm) in apoptosis; an update. Apoptosis. https://doi.org/10.1023/A:1022945107762.
- Matsuda, F., Maeda, K., Taniguchi, T., Kondo, Y., Yatabe, F., Okahashi, N., Shimizu, H., 2021. Mfapy: an open-source python package for 13C-based metabolic flux analysis. Metab. Eng. Commun. 13, e00177. https://doi.org/10.1016/j.mec.2021.e00177.
- Matsuda, F., Toya, Y., Shimizu, H., 2017. Learning from quantitative data to understand central carbon metabolism. Biotechnol. Adv. 35, 971–980. https://doi.org/10.1016/ J.BIOTECHADV.2017.09.006.
- Miyazawa, H., Yamaguchi, Y., Sugiura, Y., Honda, K., Kondo, K., Matsuda, F., Yamamoto, T., Suematsu, M., Miura, M., 2017. Rewiring of embryonic glucose metabolism via suppression of PFK-1 and aldolase during mouse chorioallantoic branching. Development (Camb.) 144, 63–73. https://doi.org/10.1242/dev.138545.
- Murakami, A., Nagao, K., Sakaguchi, R., Kida, K., Hara, Y., Mori, Y., Okabe, K., Harada, Y., Umeda, M., 2022. Cell-autonomous control of intracellular temperature by unsaturation of phospholipid acyl chains. Cell Rep. 38. https://doi.org/10.1016/ j.celrep.2022.110487.
- Niebel, B., Leupold, S., Heinemann, M., 2019. An upper limit on Gibbs energy dissipation governs cellular metabolism. Nat. Metab. 1, 125–132. https://doi.org/10.1038/ s42255-018-0006-7
- Okahashi, N., Kohno, S., Kitajima, S., Matsuda, F., Takahashi, C., Shimizu, H., 2015. Metabolic characterization of cultured mammalian cells by mass balance analysis, tracer labeling experiments and computer-aided simulations. J. Biosci. Bioeng. 120, 725–731. https://doi.org/10.1016/j.jbiosc.2015.04.003.
- Okahashi, N., Maeda, K., Kawana, S., Iida, J., Shimizu, H., 2019. Sugar phosphate analysis with baseline separation and soft ionization by gas chromatographynegative chemical ionization-mass spectrometry improves flux estimation of bidirectional reactions in cancer cells. Metab. Eng. 51, 43–49. https://doi.org/ 10.1016/j.ymben.2018.08.011.
- Okahashi, N., Yamada, Y., Iida, J., Matsuda, F., 2022. Isotope calculation gadgets: a series of software for isotope-tracing experiments in garuda platform. Metabolites 12
- Orth, J.D., Thiele, I., Palsson, B.Ø., 2010. What is flux balance analysis? Nat. Biotechnol. 28 (3 28), 245–248. https://doi.org/10.1038/nbt.1614, 2010.
- 28 (3 28), 245–248. https://doi.org/10.1038/nbt.1614, 2010.

  Ouderkirk, J.L., Krendel, M., 2014. Non-muscle myosins in tumor progression, cancer cell invasion, and metastasis. Cytoskeleton. https://doi.org/10.1002/cm.21187.
- Popovic, M., 2019. Thermodynamic properties of microorganisms: determination and analysis of enthalpy, entropy, and Gibbs free energy of biomass, cells and colonies of 32 microorganism species. Heliyon 5, e01950. https://doi.org/10.1016/j. heliyon.2019.e01950.

- Repasky, E.A., Evans, S.S., Dewhirst, M.W., 2013. Temperature matters! and why it should matter to tumor immunologists. Cancer Immunol. Res. https://doi.org/ 10.1158/2326-6066.CIR-13-0118.
- Sawai, A., Taniguchi, T., Noguchi, K., Seike, T., Okahashi, N., Takaine, M., Matsuda, F., 2025. ATP supply from cytosol to mitochondria is an additional role of aerobic glycolysis to prevent programmed cell death by maintenance of mitochondrial membrane potential. Metabolites 15, 461. https://doi.org/10.3390/ pactabol 5020461
- Si, Y., Shi, H., Lee, K., 2009. Metabolic flux analysis of mitochondrial uncoupling in 3T3-L1 adipocytes. PLoS One 4. https://doi.org/10.1371/journal.pone.0007000.
- Sousa, B., Pereira, J., Paredes, J., 2019. The crosstalk between cell adhesion and cancer metabolism. Int. J. Mol. Sci. https://doi.org/10.3390/ijms20081933.
- Tanner, L.B., Goglia, A.G., Wei, M.H., Sehgal, T., Parsons, L.R., Park, J.O., White, E., Toettcher, J.E., Rabinowitz, J.D., 2018. Four key steps control glycolytic flux in mammalian cells. Cell Syst. 7, 49–62.e8. https://doi.org/10.1016/j.cels.2018.06.003
- Thiele, I., Swainston, N., Fleming, R.M.T., Hoppe, A., Sahoo, S., Aurich, M.K.,
  Haraldsdottir, H., Mo, M.L., Rolfsson, O., Stobbe, M.D., Thorleifsson, S.G., Agren, R.,
  Bölling, C., Bordel, S., Chavali, A.K., Dobson, P., Dunn, W.B., Endler, L., Hala, D.,
  Hucka, M., Hull, D., Jameson, D., Jamshidi, N., Jonsson, J.J., Juty, N., Keating, S.,
  Nookaew, I., Le Novère, N., Malys, N., Mazein, A., Papin, J.A., Price, N.D., Selkov, E.,
  Sigurdsson, M.I., Simeonidis, E., Sonnenschein, N., Smallbone, K., Sorokin, A., Van
  Beek, J.H.G.M., Weichart, D., Goryanin, I., Nielsen, J., Westerhoff, H.V., Kell, D.B.,
  Mendes, P., Palsson, B.O., 2013. A community-driven global reconstruction of
  human metabolism. Nat. Biotechnol. 31, 419–425. https://doi.org/10.1038/
  pht 2488
- Uchiyama, S., Gota, C., Tsuji, T., Inada, N., 2017. Intracellular temperature measurements with fluorescent polymeric thermometers. Chem. Commun. 53, 10976–10992. https://doi.org/10.1039/c7cc06203f.
- Xie, Z., Bailey, A., Kuleshov, M.V., Clarke, D.J.B., Evangelista, J.E., Jenkins, S.L., Lachmann, A., Wojciechowicz, M.L., Kropiwnicki, E., Jagodnik, K.M., Jeon, M., Ma'ayan, A., 2021. Gene set knowledge discovery with Enrichr. Curr. Protoc. 1, e90. https://doi.org/10.1002/cpz1.90.
- Yang, L., Venneti, S., Nagrath, D., 2017. Glutaminolysis: a hallmark of cancer metabolism. Annu. Rev. Biomed. Eng. 19, 163–194. https://doi.org/10.1146/ annurev-bioeng-071516-044546.
- Zanotelli, M.R., Goldblatt, Z.E., Miller, J.P., Bordeleau, F., Li, J., VanderBurgh, J.A., Lampi, M.C., King, M.R., Reinhart-King, C.A., 2018. Regulation of ATP utilization during metastatic cell migration by collagen architecture. Mol. Biol. Cell 29, 1–9. https://doi.org/10.1091/mbc.E17-01-0041.
- Zhang, J., Pavlova, N.N., Thompson, C.B., 2017. Cancer cell metabolism: the essential role of the nonessential amino acid, glutamine. EMBO J. 36, 1302–1315. https://doi. org/10.15252/EMBJ.201696151.
- Zhang, R., Engel, A.L., Wang, Y., Li, B., Shen, W., Gillies, M.C., Chao, J.R., Du, J., 2021. Inhibition of mitochondrial respiration impairs nutrient consumption and metabolite transport in human retinal pigment epithelium. J. Proteome Res. 20, 909–922. https://doi.org/10.1021/acs.jproteome.0c00690.
- Zhao, R.Z., Jiang, S., Zhang, L., Yu, Z. Bin, 2019. Mitochondrial electron transport chain, ROS generation and uncoupling. Int. J. Mol. Med. https://doi.org/10.3892/ ijmm.2019.4188 (Review).
- Zielinski, D.C., Jamshidi, N., Corbett, A.J., Bordbar, A., Thomas, A., Palsson, B.O., 2017.
  Systems biology analysis of drivers underlying hallmarks of cancer cell metabolism.
  Sci. Rep. 7 (1 7), 1–14. https://doi.org/10.1038/srep41241, 2017.
- Zu, X.L., Guppy, M., 2004. Cancer metabolism: facts, fantasy, and fiction. Biochem. Biophys. Res. Commun. 313, 459–465. https://doi.org/10.1016/j.bbrc.2003.11.136.